Computational Analysis of Ducted Turbine Performance

M. Shives[1] and C. Crawford[2]

Dept. of Mechanical Engineering,
University of Victoria,
PO Box 3055, Victoria, B.C. Canada V8W 3P6

[1]E-mail: mrshives@uvic.ca
[2]E-mail: curranc@uvic.ca

Abstract

This paper studies the effects of viscous loss, flow separation and base pressure for ducted turbine designs using computational fluid dynamics (CFD) simulation. Analytical model coefficients for inlet and diffuser efficiency and base pressure coefficient parameterize these effects and have been identified from CFD results. General trends are: the inlet efficiency is nearly unity for the simulated designs; the diffuser efficiency has a significant impact on performance and is degraded by flow separation; and that the base pressure effect can provide a significant performance enhancement. Geometric features influencing each of the aforementioned parameters are identified and a regression based model is proposed for the base pressure coefficient.

Keywords: base-pressure, CFD, diffuser-augmented turbine, tidal turbine

1. Introduction

The concept of diffuser augmented turbines has been studied for decades with no commercially successful designs to date. Attempts to develop diffuser augmented wind turbines have been unsuccessful for a number of reasons; the most important of which is arguably the immense loading on the duct in storm conditions or in yawed flows. With an emerging potential for tidal turbine power generation, there is renewed interest in diffuser augmented turbines since tidal flows are typically more predictable and subject to lesser extremes than wind. There are several prototypes for vertical axis tidal turbines, however the dominant design and focus of this paper is the diffuser augmented horizontal axis tidal turbine concept.

Presently, there has been significant development of ducted turbine designs by a number of developers for capturing tidal flow energy. Despite several emerging designs, analytical models of ducted turbine performance are relatively untested and unproven. Consequently, design work relies heavily on time-consuming CFD simulation. Developing accurate analytical models would allow faster prototyping iterations during early design stages but requires empirical parameters to quantify several effects.

The rationale behind incorporating a duct is increase power by increasing the mass flow through the rotor. This is achieved by forcing an expansion of the flow downstream of the turbine. This provides a reduced pressure on the downstream side of the turbine, which acts to accelerate the flow, and therefore increases the total mass flow through the turbine. The overall effect is to increase the power produced by a given rotor diameter. The accelerated flow also allows for higher rotor rotational speeds which may result in more efficient generator operation.

A diagram of typical flow through a ducted turbine is depicted in Fig. 1. This image represents a cross-section of an axi-symmetric flow domain. The station numbers depicted in Fig. 1 are used consistently throughout this paper. The shaded section represents the rotor which is located at the duct throat.

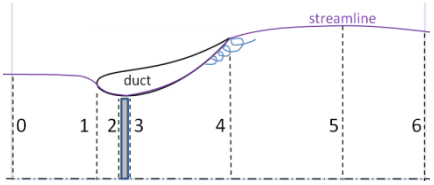

Figure 1: Stations Diagram

The mass flow increase provided by the duct is influenced by four factors: (1) the diffuser area ratio (A_4/A_2), (2) the degree of flow separation from the diffuser surface, (3) the base pressure reduction at the diffuser exit caused by obstruction of the flow, and (4) viscous losses within the entire duct. The last three of these factors are expected to vary with the operating thrust coefficient C_T.

Analytical models have been developed to characterize the performance of ducted turbines by Lawn[1], van Bussel[2] and Jamieson[3]. These models require empirical parameters which capture the effects of flow separation, base pressure, and viscous loss. At present, there is little experimental data to support a

fundamental understanding of how these factors vary with changes in duct geometry.

The models presented by Jamieson and van Bussel are based on a modified version of the standard actuator disk momentum analysis[4]. Van Bussel's model was developed to identify ideal duct performance and thus neglects viscous loss and flow separation effects. The model includes a duct expansion parameter and a base pressure speedup factor. Jamieson's model calculates an ideal zero-thrust induction factor at the rotor plane. This parameter incorporates the diffuser expansion ratio and base pressure effects (at the zero thrust condition.) Jamieson then employs an efficiency term to account for "non-ideal" duct geometry, where the ideal duct would have no flow separation, a constant base pressure coefficient and zero viscous loss. The models by Jamieson and van Bussel provide a useful extension of the standard actuator disk theory to the ducted case, but do not identify the physical parameters governing the duct performance in concrete terms.

In contrast, the model by Lawn provides a straightforward analysis of the pressure variation through the duct and identifies each major factor with a unique term. It is straightforward to identify the base pressure, flow separation and viscous effects from CFD results and to apply them to Lawn's model. This paper presents trends in the governing physical effects for ducted turbines based on seven duct designs.

2. Analytical Framework

The analytical framework for this study is based on the ducted turbine model presented by Lawn[1]. The model is developed by analyzing the variation of pressure through the duct.

From the freestream condition (p_0, u_0) the flow will undergo a contraction or expansion approaching the rotor disk plane. The variation in pressure is related to the change in velocity by Bernoulli's equation modified with an efficiency term which parameterizes viscous loss in the inlet section. Note that this definition of the efficiency is based on a flow expansion (by convention) and therefore will have values greater than unity when used for an inlet contraction with viscous loss.

$$C_{p,02} = \frac{p_2 - p_0}{\frac{1}{2}\rho u_0^2} = \eta_{02}\left[1 - \frac{u_2^2}{u_0^2}\right] \quad (1)$$

The pressure change across the actuator disk is defined according to the standard definition of the thrust coefficient. Note that Lawn defines a turbine resistance coefficient relating the thrust to the local velocity at the rotor plane (u_2) however this approach has not been followed in this analysis to facilitate a more straightforward comparison to the CFD results.

$$C_T = \frac{p_2 - p_3}{\frac{1}{2}\rho u_0^2} \quad (2)$$

The pressure change through the diffuser is found using an analogous equation to the duct inlet;

$$C_{p,34} = \frac{p_4 - p_3}{\frac{1}{2}\rho u_3^2} = \eta_{34}\left[1 - \frac{u_4^2}{u_3^2}\right] = \eta_{34}\left[1 - \frac{A_3^2}{A_4^2}\right] \quad (3)$$

where, by continuity, $u_4/u_3 = A_2/A_4$ (and $A_2=A_3$ since the actuator disk is assumed infinitesimally thin.) The pressure difference between the far wake (p_0) and the diffuser outlet is parameterized as a base pressure coefficient.

$$C_{P,b} = \frac{p_4 - p_0}{\frac{1}{2}\rho u_0^2} \quad (4)$$

Summing the pressure changes from free stream to the far wake and equating to zero, it is then possible to define the following relationships.

$$\eta_{02}\left[\left(\frac{u_2}{u_0}\right)^2 - 1\right] + C_T + C_{p,b} - C_{p,34}\left(\frac{u_2}{u_0}\right)^2 = 0 \quad (5)$$

$$\frac{u_2}{u_0} = \sqrt{\frac{\eta_{02} - C_{p,b} - C_T}{\eta_{02} - C_{p,34}}} \quad (6)$$

The overall governing equation defines the power coefficient in terms of the thrust coefficient as follows;

$$C_P = C_T \frac{u_2}{u_o} \quad (7)$$

The base pressure coefficient and efficiency terms are not generally known and need to be found experimentally or through simulations for a given duct geometry. In addition, it is expected that for a given duct, the efficiency terms and base pressure coefficient will vary as a function of thrust coefficient. The goal of this study was to validate the analytical approach taken by Lawn, to calculate the efficiency terms and base pressure coefficients over the operating range of a variety of duct designs and to identify any trends in these parameters as a function of duct geometry and operating condition.

3. Duct Geometries

To avoid making generalizations based on a single design, several duct geometries were tested. The geometric parameters expected to impact the duct performance were the diffuser expansion ratio A_4/A_3; the inlet contraction ratio A_1/A_3; the airfoil thickness ratio; and the inner and outer diffuser surface angles $\theta_{4,in}$, $\theta_{4,out}$ as depicted in Fig. 2

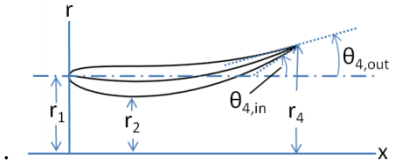

Figure 2: Geometric Attributes

Duct geometries were created following a similar methodology as presented by Hansen[5] in his CFD simulation. A baseline geometry (case 2) was designed to replicate Hansen's duct for model comparison. The duct was based on a NACA 0015 airfoil which was first scaled in thickness by a factor k_t. A camber was then applied by rotating the geometry through a linearly varying angle (0 at the leading edge to θ_1 at the trailing edge). A full body rotation through θ_2 was then applied to the entire cross section. Finally the airfoil was translated by *dr* to control the throat area A_2. These

control parameters are depicted in Fig 3. This methodology allows full control over a wide variety of duct area ratios and angles. The above control parameters and resulting duct area ratios and outlet angles are summarized in Table 1 for the seven ducts used in this study.

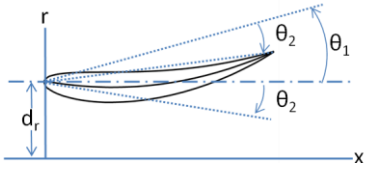

Figure 3: Control Parameters

CASE	Control Parameters				Duct Attributes			
	k_t	θ_1	θ_2	d_y	A_4/A_2	A_1/A_2	$\theta_{4,L}$	$\theta_{4,U}$
1	0.45	8.08	0.00	0.83	1.47	1.07	19.95	11.37
2	0.45	8.08	0.00	0.50	1.84	1.12	19.95	11.37
3	0.45	8.08	0.00	0.35	2.36	1.18	19.95	11.37
4	0.45	8.08	0.00	0.28	2.87	1.24	19.95	11.37
5	1.00	20.00	-18.92	0.62	1.84	1.73	27.57	10.27
6	1.00	20.00	-11.65	0.58	2.36	1.50	34.84	17.54
7	1.00	20.00	-5.00	0.56	2.87	1.34	41.49	24.19

Table 1: Control parameters & resulting attributes

Cases 1 through 4 differed only in the *dr* term and have the same exit angles and thickness ratios. This allows effects due to changing the area ratios to be isolated. Cases 5 through 7 were designed such that the diffuser outlet angles increase as the diffuser expansion ratio increases. The diffuser outlet angle for cases 5-7 were set to correspond to those for cases 2-4; allowing effects due to the outlet angles to be observed. It is realized that this does not represent a full search space for all duct parameters – however the intent of this study is to identify some general trends, and not to define a universal model for all possible ducts.

4. CFD Simulation

CFD simulations were carried out using ANSYS CFX, following a similar methodology to that of Hansen[5]. The simulations use an axi-symmetric actuator disk model without swirl to produce results that are readily used to calculate the efficiency and pressure coefficient terms of the analytical model. The mesh is a 15° slice of the entire flow domain. Periodic boundary conditions were enforced to simulate the entire 360° domain. This mesh was realized by sweeping a 2D structured surface mesh through a 15° rotation in five elements. The mesh is refined in proximity to the duct surface and actuator disk. The turbulence was modeled using the k-ω SST option due to its good performance in predicting boundary layer separation with adverse pressure gradients. No model for the transition from laminar to turbulent flow was used as the flow is expected to be turbulent along the entire duct surface.

Distances were non-dimensionalized based on the duct length L. The inlet was 5L upstream of the duct leading edge and employed a uniform velocity. The outlet is 10L downstream of the trailing edge and enforces $p=p_0$. As in Hansen[5] an inner radial boundary employing a free-slip condition was located at 0.05L to avoid a singularity in azimuthal velocity at the centerline. The outer radial boundary is located at r=5L and was treated using the opening for entrainment option, which approximates an infinite domain. The sensitivity of the simulated C_P to moving the outer radial boundary to 10L was less than 1%; this was considered acceptable.

The actuator disk is simulated as a momentum sink where a force per unit volume f_x is applied at each element. The disk is located at the duct throat. The force distribution is uniform over the actuator disk. The f_x term was calculated based on the actuator disk thickness and the desired thrust coefficient for each simulation. To be consistent with the simulation by Hansen, a small gap of width $0.08r$ was left between the outer radius of the actuator disk and the surface of the duct. As shown by Hansen, this gap accelerates the boundary layer flow and is thought to delay flow separation. This effect would not be present in a real turbine with a discrete number of blades unless the solidity ratio was very high. The gap was used nonetheless to maintain consistency with Hansen for subsequent validation.

The actuator disk CFD methodology has been validated for the non-ducted rotor case and was found to reproduce the standard actuator disk theory well as shown in Fig. 4. (Note that the Glauert empirical thrust correction[4] with $C_{T,1}$=1.7 is applied to the theory curve for $C_T > \frac{8}{9}$ to account for momentum theory breakdown at high thrust).

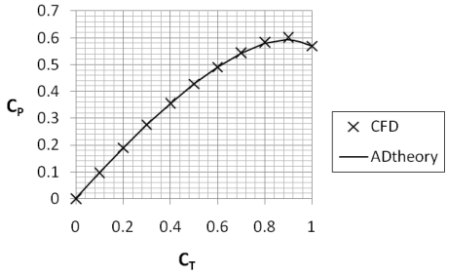

Figure 4: Comparison of CFD method to actuator disk theory

4.1 Grid Refinement Study

To ensure minimal grid resolution error, the effect of grid refinement on the power coefficient and rotor plane induction was studied using the baseline duct geometry. Adequate resolution of the boundary layer along the duct was considered crucial. It was found that the simulated power coefficient varied nearly linearly with the 1st layer spacing in the boundary layer region. A sample plot is shown in Fig. 5 for C_T 0.9. The linear trend was used to determine the expected C_P with an infinitesimally small spacing. This allowed a calculation of the expected resolution error for each mesh. The final mesh had a 1st layer spacing of 0.08 mm and the expected error in C_P was less than 1% for C_T ranging from zero to one. This mesh spacing gave a y^+ value less than 10 at all points along the duct.

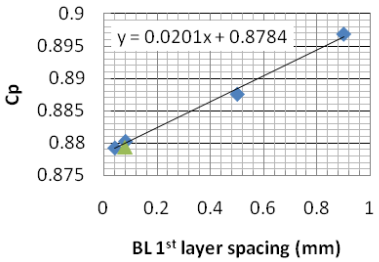

Figure 5: Effect of boundary layer mesh size on C_P

The same strategy was used to study the axial spacing, which was refined at the duct inlet, outlet, and at the rotor plane. It was found that with a minimum axial spacing of 0.5 mm at the trailing edge, the expected C_P error was less than 1% over the full range of C_T. The final mesh consisted of 467 elements in the axial direction, 43 elements crossing the boundary layer refinement O-grid, and 142 elements in the radial direction. The total number of elements was 313 530.

4.2 CFD comparison to Hansen

The baseline duct geometry was a replica of that simulated by Hansen. As a validation of the CFD model, the C_P-C_T relationship was compared to Hansen's result as shown in Fig. 6. The maximum C_P in the present simulations is 3% lower than Hansen's result. This discrepancy is likely due to minor differences in duct geometry and meshing strategy, but is considered acceptable.

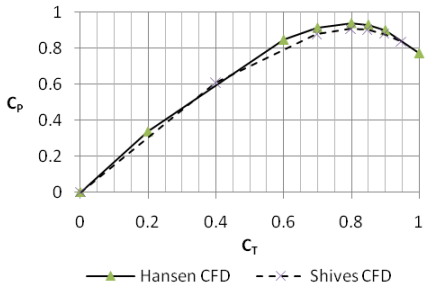

Figure 6: Comparison to Hansen's result.

5. Results

The thrust was calculated as the volume integral of f_x over the actuator disk and normalized by $\frac{1}{2}\rho u_0^2$ to give C_T. This calculation validated that the specified f_x produced the desired C_T. Similarly, the power was found as the volume integral of uf_x over the disk and normalized by $\frac{1}{2}\rho u_0^3$ to give C_P. A streamline passing through the leading edge stagnation point and the duct trailing edge was defined to isolate the flow passing through the duct. Planes were then defined at stations 0 through 6 bounded by the streamline. This allowed calculation of the area-averaged velocity, pressure, and stagnation pressure at each station. These area-averages were then used to calculate the model parameters as described in sections 5.2-5.4.

5. 1 C_P vs. C_T

The power coefficient is plotted as a function of C_T for all ducts in Fig. 7. The first four duct designs maintained a constant diffuser outlet angle of 19° while changing the duct expansion ratio. The effect of this was as expected for cases 1 to 3, with larger expansion resulting in greater C_P enhancement; however case 4 showed no further improvement over case 3 as the area ratio increased from 2.36 to 2.87. The flow field for ducts 3 and 4 operating at C_T=0.9 is depicted in Fig. 8. The region of separated flow (where u<0) is shown in black. It is expected that at a given diffuser angle, the maximum performance enhancement possible by increasing the expansion ratio is limited by flow separation effects.

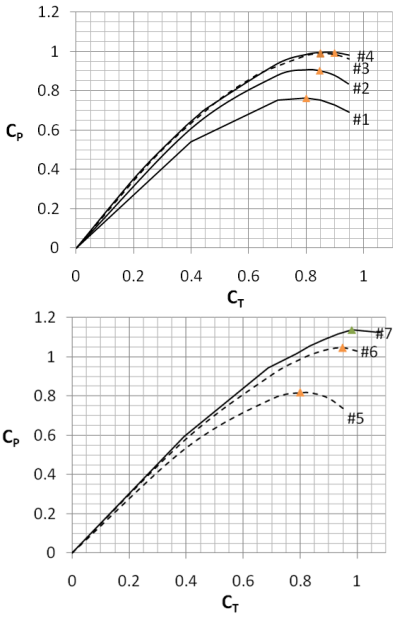

Figure 7: Performance characteristic for each duct

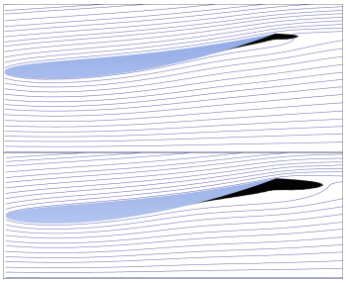

Figure 8: Flow separation at C_T=0.9; duct 3 (top) and 4 (bottom)

The next set of ducts (cases 5-7) was created to test the impact of outlet angle on performance. It was seen that by increasing the duct outlet angle as the area ratio grew, greater performance enhancements were possible. It is thought that large outlet angles provide a greater base pressure effect due to blockage of the flow exterior to the duct. This effect competes with the performance reduction seen with greater flow separation at large area ratios.

Flow separation essentially creates a smaller core flow, reducing the effective expansion by the diffuser. A large base pressure effect acts to delay flow separation by reducing the adverse pressure gradient experienced by the flow through the diffuser. This

occurs because some of the pressure recovery to ambient takes place downstream of the diffuser exit.

5. 2 Inlet efficiency

The inlet efficiency was found using eq. 8. Note that the efficiency term is very sensitive to discrepancies in the pressure when u_2 approaches u_0, which occurs at a specific C_T for each duct when the freestream ingested flow area equals the rotor area.

$$\eta_{02} = \frac{p_2 - p_0}{\frac{1}{2}\rho(u_0^2 - u_2^2)} \quad (8)$$

This sensitivity was avoided by assuming that the efficiency calculated for C_T=0 was appropriate for all values of C_T. The inlet efficiency was not expected to show significant variation with C_T because unlike in the diffuser, flow separation is very unlikely in the inlet and the efficiency is primarily due to friction over a relatively constant surface. Assuming constant inlet efficiency produced a good agreement between the simulated C_P and that calculated by Lawn's method. It was seen that the inlet efficiency was typically within 2% of unity and that simply assuming a value of unity had little effect on the calculated C_P.

5. 3 Diffuser efficiency

The diffuser efficiency calculated from eq. 9 accounts for viscous loss and flow separation. The diffuser efficiency is plotted in Fig. 9 for all ducts.

$$\eta_{34} = \frac{p_4 - p_3}{\frac{1}{2}\rho u_3^2\left[1 - \frac{A_3^2}{A_4^2}\right]} \quad (9)$$

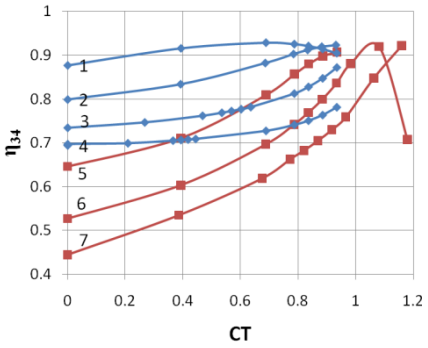

Figure 9: Diffuser Efficiency

It was observed that as (A_4/A_2) and $\theta_{4,IN}$ grow, the diffuser efficiency diminishes due to increasing flow separation. As the thrust coefficient rises, there is less flow separation and the diffuser efficiency rises. This behaviour is likely due to the fast flowing jet created in the gap between the duct and the edge of the actuator disk. The jet becomes stronger at higher thrust, energizing the boundary layer and delaying flow separation. It is realized that such a jet may not occur in real turbines unless the solidity ratio is very high or other design features lead to its presence. This discrepancy may result in an over-prediction of the maximum C_P. Work is ongoing to test the sensitivity of the simulated C_P to the gap.

5. 4 Base pressure coefficient

The base pressure coefficient was calculated from eq. 4 and is plotted in Fig. 10. The base pressure coefficient was seen to increase in magnitude with (A_4/A_2) and $\theta_{4,OUT}$. As seen in Fig. 10, the base pressure coefficient was seen to decrease in magnitude as the thrust coefficient increases.

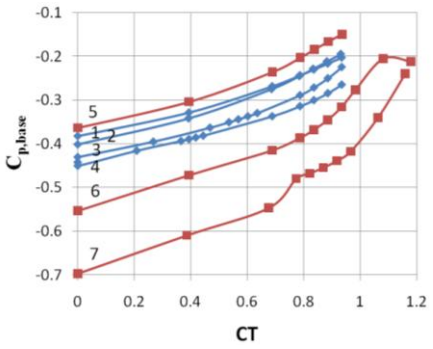

Figure 10: Base pressure coefficient

5.6 Regression based correlations

An attempt was made to parameterize the diffuser efficiency and base pressure as functions of duct geometry and thrust coefficient. The general strategy taken was to first model these coefficients at the zero-thrust condition, then to parameterize the trends with varying CT.

The diffuser efficiency and base pressure at the zero thrust condition ($\eta_{34,0}$, $C_{P,b0}$) were fit using linear regression techniques. The duct efficiency was found to be a function of (A_2/A_4) and $\theta_{4,IN}$ according to eq. 10 with a_1=0.551, b_1=-0.0121, c_1=0.729. This equation was within 5% of the simulated value for the ducts in this study.

$$\eta_{34,0} = a_1\frac{A_3}{A_4} + b_1\theta_{4IN} + c_1 \quad (10)$$

In a similar manner, the zero-thrust base pressure coefficient was found to correlate to (A_2/A_4) and $\theta_{4,OUT}$ according to eq. 11. With a_2=0.186, b_2=-0.0194, c_2=-0.286. This correlation was within 6% of the simulated value for all ducts in this study.

$$C_{p,b0} = a_2\frac{A_3}{A_4} + b_2\theta_{4OUT} + c_2 \quad (11)$$

The above correlations show that the efficiency term is reduced as the inner exit angle ($\theta_{4,IN}$) increases – this equation makes physical sense because at larger angles, there will be increased flow separation. The base pressure coefficient on the other hand, will grow in magnitude as the outer exit angle ($\theta_{4,OUT}$) increases. Therefore it may be desirable to incorporate a split-flap style trailing edge such as the 'brim' design of Setoguchi[6] into future duct designs to maximize the base pressure effect while limiting the flow separation.

The variation of the base pressure coefficient with C_T was modelled as a linear function where the slope depends on the diffuser outer exit angle. This allowed the base pressure to be defined as in eq. 12 with a_3=0.006 and b_3=0.150.

$$C_{p,b} = C_{b,p0} + (a_3\theta_{4,OUT} + b_3)C_T \quad (12)$$

Attempts to model the variation of the diffuser efficiency with C_T did not produce useful correlations.

However there is significant empirical data in literature for duct expansion C_P values which could provide the basis for an empirical model.

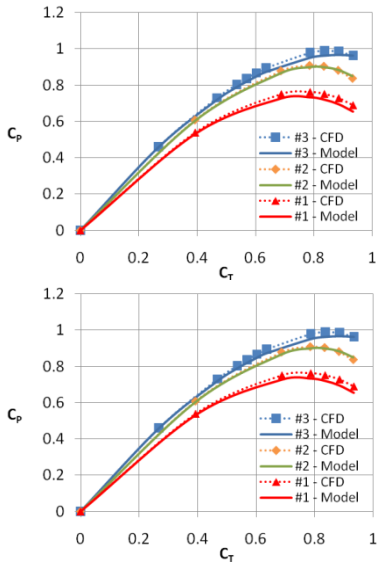

Figure 11: C_P calculated using the base pressure model

Using the base pressure coefficient from eq. 12, an inlet efficiency of unity and the diffuser efficiency derived from CFD results, eq. 6-7 were used to calculate the C_P over the range of C_T for each duct. A comparison to the CFD results is shown in Fig 11. Qualitatively, the base pressure coefficient model provides a good match to the CFD result. As with any regression based model, a separate dataset from that used to derive the model should be used for validation. More simulations with new geometries are required for this purpose.

6. Discussion

Using a validated CFD modelling approach, several duct designs were simulated with an actuator disk representation of the turbine. These simulations provide insight into the factors influencing the performance enhancement provided by ducts; viscous loss, flow separation and base pressure. It was found that viscous loss in the inlet had only a small impact on the power for the tested designs. Flow separation of the boundary layer in the diffuser section leads to significant performance degradation while the base pressure effect provides a significant enhancement. For the ducts in this study, flow separation was reduced as C_T increased This is thought to be due to the fast flowing jet through the gap between the actuator disk and duct energizing the boundary layer. The base pressure coefficient on the other hand had a diminishing effect as C_T increased. An empirical model for the base pressure was derived which provides a good match to the CFD results. Due to the limited range of duct geometries studied, the relationships derived here are not expected to be applicable to ducts with very different geometries. The general trend that diffuser efficiency varies with the inner diffuser exit angle and the diffuser expansion ratio is expected to be valid over a wide variety of ducts. Similarly, it is expected that for most ducts, the base pressure coefficient will vary with the diffuser outlet angle and the expansion ratio. For split-flap style exits the base pressure will likely be related to the ratio of the throat area to the total area at the exit (i.e. the duct exit area plus the area blocked by the flap). Future work will examine this fuller range of geometries in more detail, continue to explore analytic models with appropriate parameterised constants and look at the effects of individual blades.

Acknowledgements

The authors acknowledge the National Sciences and Engineering Research Council (NSERC) of Canada and the University of Victoria for financial support.

References

[1] C.J. Lawn. (2003): Optimization of the power output from ducted turbines. Pp 107-117. Proc. Instn Mech. Engrs Vol. 217 Part A: J. Power and Energy.

[2] G.J. van Bussel. (2007): The science of making more torque from wind: Diffuser experiments and theory revisited. Pp 1-12. Journal of Physics: Conference Series, Vol. 75.

[3] P. Jamieson. (2008): Generalized Limits for Energy Extraction in a Linear Constant Velocity Flow Field. Pp 445-457: Wind Energy, Vol. 11.

[4] T. Burton, D. Sharpe, N. Jenkins. E. Bossanyi. (2001): Wind Energy Handbook. Pp 43-67: John Wiley and Sons.

[5] M.O.L. Hansen., N.N. Sorensen., R.G.J. Flay., (2000): Effect of Placing a Diffuser around a Wind Turbine, Pp 207-213: Wind Energy, Vol 3

[6] T. Setoguchi, N. Shiomi, K. Kaneko., (2004): Development of two-way diffuser for fluid energy conversion system. Pp 1757-1771: Renewable Energy, Vol 29